ISSN 1349-1113
JAXA-RR-06-042E

JAXA Research and Development Report

Inviscid Numerical Simulations of 2D Parallel Blade-Vortex Interaction JAXA / ONERA Cooperation

Y. TANABE, S. SAITO, C. YANG and T. AOYAMA
C. BENOIT, J.-O. GRETAY, G. JEANFAIVRE, S. PERON and J. SIDES

March 2007

Japan Aerospace Exploration Agency

JAXA-RR-06-042E

JAXA Research and Development Report

Inviscid Numerical Simulations of 2D Parallel Blade-Vortex Interaction JAXA / ONERA Cooperation

Y. TANABE*1, S. SAITO*1, C. YANG*1 and T. AOYAMA*1
C. BENOIT*2, J.-O. GRETAY*2, G. JEANFAIVRE*2, S. PERON*2 and J. SIDES*2

*1 JAXA
*2 ONERA

March 2007

Japan Aerospace Exploration Agency

Inviscid Numerical Simulations of 2D Parallel Blade-Vortex Interaction JAXA / ONERA Cooperation

Y. TANABE *1, S. SAITO *1, C. YANG *1 and T. AOYAMA *1
C. BENOIT *2, J.-O. GRETAY *2, G. JEANFAIVRE *2, S. PERON *2 and J. SIDES *2

ABSTRACT

Inviscid numerical simulations of two-dimensional parallel blade-vortex interaction are carried out in the framework of Task 1 (1st year) of the cooperative research activity between JAXA and ONERA on the "Comparison of CFD and BVI noise prediction methods for realistic rotors". The capability of respective JAXA and ONERA Euler methods for an accurate capture of main features of parallel Blade-Vortex Interaction is evaluated. The results from each side are compared quite well to each other and with NASA experiments with the main features well captured. But some discrepancies are found mainly due to different numerical schemes and computation approaches adapted by each organization.

Keywords : JAXA/ONERA, Helicopter noise, BVI, CFD simulation

要　約

JAXAとONERAの共同研究である"実在ロータに関するCFDとBVI騒音予測方法の比較研究"のタスク1として、2次元のブレード・渦干渉（BVI）の非粘性数値シミュレーションが実施された。JAXAとONERAが保有するそれぞれのEulerコードがパラレルBVIの主な特徴を正確に捕捉する能力について評価を行った。両機関のシミュレーションの結果は互いに比較を行い、NASAの実験とも比較され、主な点についてはほぼ一致していることが分かった。それぞれが使用した数値スキームと計算手順の違いにより、結果においてはいくつかの差異があることも分かった。

Nomenclature

α	airfoil incidence
γ	ratio of specific heats
μ	rotor advance ratio
Ω	rotor rotational speed
c	blade section
c_{vg}	vortex generator chord
M_∞	freestream Mach number in the 2D CFD study
M_{tip}	hover tip Mach number in the experiment
p_∞	freestream pressure
R	rotor radius
r	blade spanwise coordinate
$V_{\infty exp}$	local freestream velocity in the experiment
V_∞	freestream velocity in the 2D CFD study
v_θ	tangential velocity of the vortex
x	dimensionless blade chordwise coordinate
x_0	vortex core initial X-coordinate
y_0	vortex core initial Y-coordinate
Γ_v	nondimensional vortex circulation
ρ_∞	density at the freestream conditions
ζ_v	nondimensional vortex core radius (ratio of maximum tangential velocity radius / vortex generation chord)

*1 JAXA
*2 ONERA

Introduction

Background

Helicopters are playing more important roles in human activities. Using helicopter for emergency medical service (EMS) and doctor delivering onto the highway or other life saving site proved to be very effective and the number of so-called doctor-helicopter is increasing in Japan and Europe as well. Because the operation of helicopter over the urban areas becomes more frequent, the complaints about the helicopter noise often annoy the helicopter operators and seriously restrict the new heliport settlement in the urban area especially in Japan.

New helicopter design criteria for reduced noise level are strengthening time by time. Current newly developed helicopters usually have lower noise signature than older ones when flying over, but the so-called slap noise occurs when helicopter is in descending flight during the landing approach still remains an annoying problem. This noise is caused by the interaction between the rotor blade with its own wake, known as blade tip-vortices. The blade-vortex interaction (BVI) causes impulsive airload change on the blade and also impulsive noise. To reduce the BVI thus reduce the vibration and noise, several active control techniques are proposed and under research and development. The understanding of the BVI phenomena and accurate simulation is a key for the design of such technologies.

Computational fluid dynamics (CFD) technologies have been widely used for the fixed wing aircraft design but only recently began to be applied to the complicated rotary wings. A concentrated vortex core causes higher impulsive noise levels, and these higher levels are diminished for a diffused vortex core. Maintaining the size and strength of a vortex core is then important for capturing BVI with CFD methods. How many grids are required to resolve a vortex core without diffusing are highly numerical schemes dependent. So comparison of the CFD results obtained with different numerical methods for a common test case is a very efficient and instructive way for the development and improvements of reliable prediction tools.

Context of the study

This work has been achieved in the framework of Task 1 (1st year) of the cooperative research activity between JAXA and ONERA on the “Comparison of CFD and BVI noise prediction methods for realistic rotors”. The goal of Task 1 is to evaluate the capability of respective JAXA and ONERA Euler methods for an accurate capture of main features of parallel Blade-Vortex Interaction. To achieve this task, a time-accurate simulation of the interaction between an analytical vortex and a two-dimensional airfoil is performed. The initial steady flow conditions around the airfoil are chosen as representative of a typical BVI event on a helicopter rotor. The vortex is introduced 10 chords upstream from the leading edge of the airfoil to check the effects of numerical diffusion during the advection phasis of vortices over a large distance.

Content of the report

In this report, the chosen test case is first described in section 1, JAXA and ONERA numerical methods are presented in section 2, and in section 3 analysed data extracted from the simulation are presented. Then the study is mainly split into two parts: in the first part (section 4) a grid refinement study is performed, the flow using JAXA 4th-order and ONERA 2nd-order Euler solvers is computed on a sequence of finer and finer meshes. Analysis of solution and comparison with the experiment are provided and results are compared (JAXA studies versus themselves, ONERA studies versus themselves and JAXA and ONERA studies versus NASA experiment) and critically analysed. In the second part (section 5), high-order spatial discretisation schemes recently developed at ONERA are used for computing the BVI test-case on a given reference mesh, and comparisons with the previous results are performed.

1 Test case

The test case is chosen in order to be both realistic and comparable with an experiment carried out by Caradonna et al. in [1], which implies that the vortex should be located approximatively 0.25 chord below the profile and clockwise-rotating.

1.1 Choice of the test case

According to the given requirements in introduction, the selected test-case is the one similar to the A-5 experi-

ment in [2]. The characteristics are the following ones:

$$\begin{cases} M_{tip} = 0.714 \\ \alpha = 0° \\ \mu = 0.198 \\ y_0 = -0.25\,c \end{cases}$$

Although the main goal of the task is to compare the JAXA and ONERA Euler solutions, the computations should be compared with the experiment. In the experiment, the interaction between the vortex and the blade occurs when the rotor is in the axis of the wind tunnel. Hence the velocity of the vortex towards the blade is, in a two-dimensional plane, the velocity of the point of the rotor where is studied the interaction. The experimental tip Mach number is M_{tip} = 0.714, and experimental data are located at r/R = 0.876, which leads to a local Mach number M_∞ in the computation defined by:

$$M_\infty = M_{tip} \times \frac{r}{R} = 0.626$$

1.2 Dimensional analysis

The variables are nondimensionalized with respect to distance, velocity and density in the following manner:

- distances are nondimensionalized with respect to the blade chord: c = 1.
- velocities are nondimensionalized with respect to the freestream velocity: V_∞ = 1.
- densities are nondimensionalized with respect to ρ_∞ : ρ_∞ = 1.

$$\text{Hence: } p_\infty = \frac{1}{\gamma M_\infty^{\,2}}, \text{ and: } \left.\begin{aligned} V_\infty &= \Omega R \times \tfrac{r}{R} \\ V_{\infty exp} &= \mu\,\Omega\,R \end{aligned}\right\} \Rightarrow V_{\infty exp} = \frac{\mu \times V_\infty}{r/R}$$

- time is nondimensionalized with respect to c/V_∞, so the vortex moves 1 chord length at 1 nondimensional time. Time is shifted so that t=0 is the vortex core center under the airfoil nose.

1.3 Vortex model and parameters

The vortex is created using the Scully algebraic model, which is the best vortex core model according to the experiment. With this model, the tangential velocity equation in the vortex frame in dimensionless form is expressed by:

$$v_\theta(r) = \frac{\Gamma_v}{2\pi} \frac{r}{r^2 + \zeta_v^2}, \text{ where:}$$

$$\Gamma_v = 0.374\, V_{\infty exp}\, c_{vg} = 0.374\, \frac{\mu\, V_\infty}{r/R}\, c_{vg}, \text{ and } \zeta_v = 0.054\, c_{vg}.$$

Thus the advection velocity of the vortex is M_∞ = 0.626,

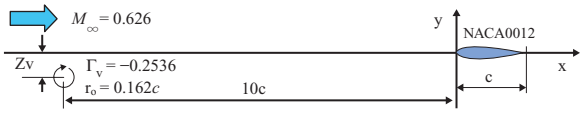

Figure 1: Test case selected for comparision (Zv=-0.25c)

the vortex circulation is Γ_v = 0.2536 and the core radius is ζ_v = 0.162. The vortex is initially located at (x_0, y_0) = (-10., -0.25) (see figure 1).

2 Numerical study

The numerical approach used in ONERA is Chimera method while in JAXA is overlapped grids approach. Both use Cartesian grids as backgrounds to resolve the vortex and body fitted curvilinear grids for the airfoil. The methods used to ensure geometric connectivity between these grids are different from each other. The Chimera method only interpolates the overlapped boundary points from the inner grid onto the background grid, while in the overlapped grids approach, the whole area of the inner grids are interpolated onto the background.

To preserve the temporal and spatial accuracy across the grid boundaries for unsteady flow, explicit schemes are generally used for the background Cartesian grid with small CFL number (less than 1) for both methods. With suitable overlapped boundary width matched with the numerical scheme stensil length, Chimera method is identical with the overlapped grids approach numerically. The advantage of the Chimera method is possible significant reduction of the interpolation points but requires to keep the hole-cutting with a suitable stensil width depending on the numerical schemes used. With suitable coverage of the inner blade grid, overlapped grids approach offers a more robust and simpler means for the overset grids computations.

2.1 ONERA CFD Methods

The characteristics of the computational Euler method used at ONERA for this study are the following ones:

- Multiblock structured grid approach,
- Chimera tools (see [4]-[5]),
- Time-stepping scheme for background Cartesian grids:
- 4-stage Runge-Kutta time-stepping scheme for unsteady flow,
- backward Euler time-stepping scheme for initial steady flow.

- Implicit stages for airfoil curvilinear grid:
- Implicit Residual Smoothing for unsteady flow (see [6]),
- Implicit LDU for initial steady flow (see [8]),

Three spatial discretization schemes are used here:

1. a 2nd-order space-centered scheme based on Jameson's scheme, referred later as "2nd-order" (see [7]), using:
- a Finite Volume formulation ,
- a 2nd-order nonlinear artifficial viscosity, with $k_2 = 0$,
- a 4th-order artifficial viscosity, with $k_4 = 0.016$,
- a CFL number for steady computations $CFL = 40$.

2. a 3rd-order space-centered scheme on both Cartesian and curvilinear grids (see [9],[10]), referred later as "3rd-order", using:
- a Finite Volume formulation on curvilinear grids, a Finite Difference approach on Cartesian grids ,
- a 2nd-order nonlinear artifficial viscosity, with $k_2 = 0$,
- a 4th-order artifficial viscosity, with $k_4 = 0.016$,
- a CFL number for steady computations $CFL = 10$.

3. a 5th-order space-centered scheme on Cartesian grids and 3rd-order space-centered scheme on curvilinear grids, referred later as "5th-order", using:
- a 3rd-order numerical scheme on curvilinear grids similar to 2 and a Finite Difference approach on Cartesian grids (see [10]) ,
- a 6th-order artifficial viscosity, with coefficient $k_4 = 1/60$ for Cartesian grids ,
- a CFL number for steady computations $CFL = 10$.

Corresponding values of time steps used in unsteady computations are presented further in section 2.5. Chimera interpolations are of a 2nd-order of accuracy for 2nd-order computations, and of a 3rd-order of accuracy for higher-order computations.

The stencil is corrected for one layer of interpolated cells at overlap borders and at the fringe of blanked cells, in order to get 2nd-order formulations locally.

2.2 JAXA CFD Methods

The numerical characteristics of the computational code used at JAXA for this study are the following ones:
- Moving Overlapped Grids Approach (see [11]),
  - Exchange information between grids at pre-designated time step,
  - Divided time steps for each grid to meet each maximum CFL.
- Cartesian Background Grids (inner and outer),
  - Euler solver,
  - 4th-order spatial accuracy, SHUS scheme (see [12]),
  - 4-stage Runge-Kutta explicit time integration (better than 2nd-order time accuracy),
  - $CFL \leq 0.8$ for this study.
- Moving blade grid (fixed in this study),
  - NS solver (use Euler only at this study),
  - 2nd-order spatial accuracy, Harten & Yee's TVD scheme (see [13]),
  - Implicit time integration, 1-stage, 2nd-order conservative form,
  - $CFL \leq 25$ for this study.

2.3 ONERA computational domain

2.3.1 General properties

The mesh is generated in order to be fine along the path of the vortex and near the profile, coarse far from the profile and outside the vortex path. It is built in order to model large enough a domain (to prevent from boundary effects) and to get a reasonable computational time.

The Chimera approach is performed here, with one layer of interpolated cells at the fringe of blanked cells and at overlap boundary conditions. It enables:
- the use of a curvilinear mesh close to the profile, and regular Cartesian grids elsewhere, and thus a reduction of the computational cost.
- refinements of the mesh in subzones as described below,
- an optimization of the parallel computation by splitting the domain in different zones.

The different zones of the mesh are depicted in figure 2. The global mesh consists of a curvilinear body grid and of 12 Cartesian grids. The 4 grids close to the profile (red grids on figure 2) have matching boundary with one another, and overlap boundary conditions with their respective adjacent grids. Overlap boundary conditions are applied to remaining Cartesian grids in overlap regions. Four different meshes have been generated to compare the results and to make a grid refinement study. It should be enhanced that the number of cells in the vortex core radius is a major parameter for the simulation of parallel blade-vortex interaction.

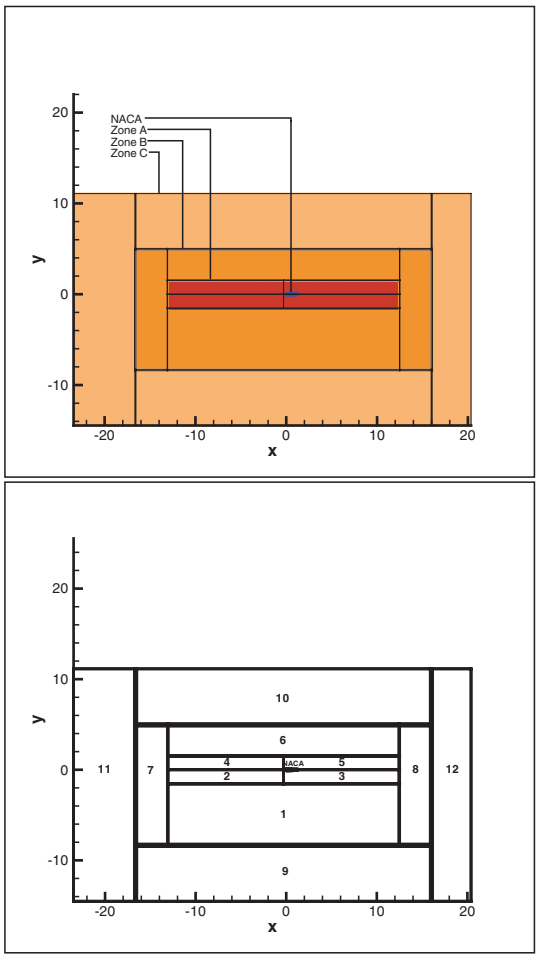

Figure 2: Global mesh: zones and subzones (ONERA).

2.3.2 Cartesian Mesh

The Cartesian mesh is made of three main zones, any of them being the union of 4 subzones with the same cell-edge length:

- zone A is the zone in which the mesh is the most refined (center of the domain: subzones 2, 3, 4, 5),
- zone B is the zone in which the mesh is medium (subzones 1, 6, 7, 8),
- zone C is the zone in which the mesh is the coarsest mesh (subzones 9, 10, 11, 12).

Cell-length ratio between zones A and B, and between zones B and C is 1/3. Thus, the area of a cell in zone B is 9 times larger than the area of a cell in zone A, and the area of a cell in zone C is 9 times larger than the area of a cell in zone B.

2.3.3 NACA0012 Mesh

The body mesh of the NACA0012 profile is refined near the body and at the leading and trailing edges. The mesh size when moving away from the body is increasing as a hyperbolic tangent function which, according to [3], is the best function for meshing near walls. The NACA0012 mesh used for the reference case is presented in figures 3 and 4 .

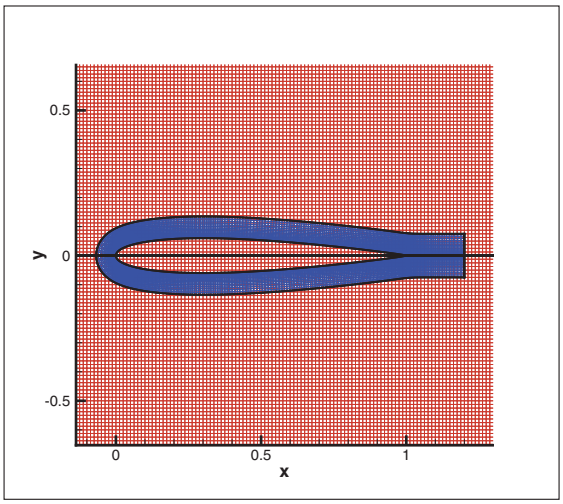

Figure 3: NACA0012 mesh: global view of the reference body grid.

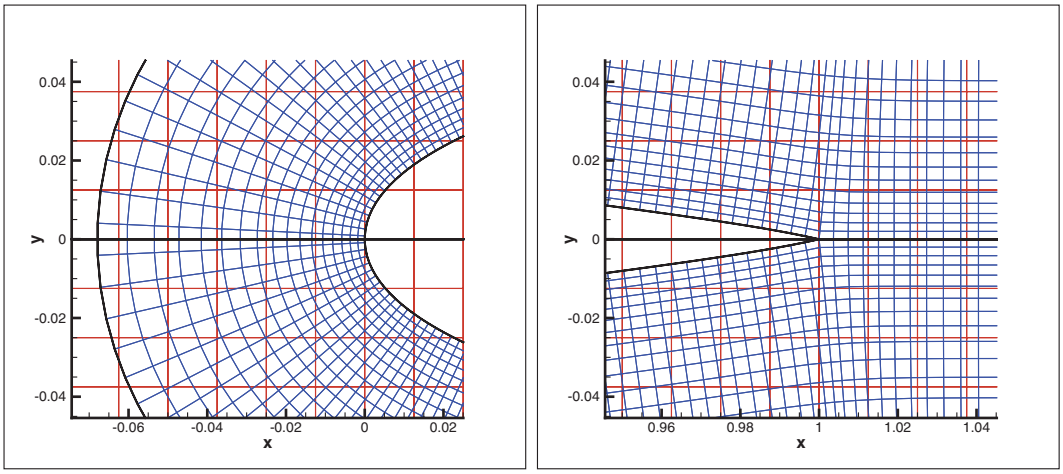

Figure 4: NACA0012 mesh: close-up views near the leading edge and trailing edge (reference grid).

2.3.4 Chimera meshing

Given this configuration, the body grid oversets Cartesian grids 3 and 5. As introduced in section 2.3.1, grids 2, 3, 4 and 5 have matching boundaries with one another. Anywhere else, overlap boundary conditions are applied, with at least 2 cells of a grid overlapping another grid.

2.3.5 Meshes

Study1: Reference Cartesian mesh + Reference body mesh. This mesh is made in order to have 13 cells in the vortex core radius. The global mesh is made of 842777 cells distributed as following:

Zone	Cell − egde	x_{min}, y_{min}	x_{max}, y_{max}	x × y	Cells
1	0.0375	(− 13.125, − 8.4375)	(12.525, − 1.5)	684 × 185	126540
2	0.0125	(− 13.125, − 1.575)	(− 0.3, 0.)	1026 × 126	129276
3	0.0125	(− 0.3, − 1.575)	(12.525, 0.)	1026 × 126	129276
4	0.0125	(− 13.125, 0.)	(− 0.3, 1.575)	1026 × 126	129276
5	0.0125	(− 0.3, 0.)	(12.525, 1.575)	1026 × 126	129276
6	0.0375	(− 13.125, 1.5)	(12.525, 5.0625)	684 × 95	64980
7	0.0375	(− 16.725, − 8.4375)	(− 13.05, 5.0625)	98 × 360	35280
8	0.0375	(12.45, − 8.4375)	(16.125, 5.0625)	98 × 360	35280
9	0.1125	(− 16.725, − 14.5125)	(16.125, − 8.2125)	292 × 56	16352
10	0.1125	(− 16.725, 4.8375)	(16.125, 11.1375)	292 × 56	16352
11	0.1125	(− 23.475, − 14.5125)	(− 16.5, 11.1375)	62 × 228	14136
12	0.1125	(15.9, − 14.5125)	(20.4, 11.1375)	40 × 229	9120
NACA	0.0017 *to* 0.0117	(− 0.068, − 0.135)	(1.2, 0.135)	449 × 17	7633
Global		**(− 23.475, − 14.5125)**	**(20.4, 11.1375)**		**842777**

Study2: Reference Cartesian mesh + Refined and enlarged body mesh. This study is the same as Study1, but with a refined and enlarged NACA0012 mesh. The Cartesian mesh is made in order to have 13 cells in the vortex core radius. The global mesh is made of 881911 cells distributed as following:

Zone	Cell − egde	x_{min}, y_{min}	x_{max}, y_{max}	x × y	Cells
1	0.0375	(− 13.125, − 8.4375)	(12.525, − 1.5)	684 × 185	126540
2	0.0125	(− 13.125, − 1.575)	(− 0.3, 0.)	1026 × 126	129276
3	0.0125	(− 0.3, − 1.575)	(12.525, 0.)	1026 × 126	129276
4	0.0125	(− 13.125, 0.)	(− 0.3, 1.575)	1026 × 126	129276
5	0.0125	(− 0.3, 0.)	(12.525, 1.575)	1026 × 126	129276
6	0.0375	(− 13.125, 1.5)	(12.525, 5.0625)	684 × 95	64980
7	0.0375	(− 16.725, − 8.4375)	(− 13.05, 5.0625)	98 × 360	35280
8	0.0375	(12.45, − 8.4375)	(16.125, 5.0625)	98 × 360	35280
9	0.1125	(− 16.725, − 14.5125)	(16.125, − 8.2125)	292 × 56	16352
10	0.1125	(− 16.725, 4.8375)	(16.125, 11.1375)	292 × 56	16352
11	0.1125	(− 23.475, − 14.5125)	(− 16.5, 11.1375)	62 × 228	14136
12	0.1125	(15.9, − 14.5125)	(20.4, 11.1375)	40 × 229	9120
NACA	0.0001 *to* 0.0057	(− 0.096, − 0.16)	(1.2, 0.16)	917 × 51	46767
Global		**(− 23.475, − 14.5125)**	**(20.4, 11.1375)**		**881911**

Study3: Refined Cartesian mesh + Refined body mesh. This study is the same as Study1, but with refined Cartesian and NACA0012 meshes. The Cartesian mesh is made in order to have 26 cells in the vortex core radius. The global mesh is made of 3284675 cells distributed as following:

Zone	Cell − egde	x_{min}, y_{min}	x_{max}, y_{max}	x × y	Cells
1	0.01875	(− 13.0875, − 8.325)	(12.4875, − 1.5)	1364 × 364	496496
2	0.00625	(− 13.0875, − 1.5375)	(− 0.3, 0.)	2046 × 246	503316
3	0.00625	(− 0.3, − 1.5375)	(12.4875, 0.)	2046 × 246	503316
4	0.00625	(− 13.0875, 0.)	(− 0.3, 1.5375)	2046 × 246	503316
5	0.00625	(− 0.3, 0.)	(12.4875, 1.5375)	2046 × 246	503316
6	0.01875	(− 13.0875, 1.5)	(12.4875, 4.95)	1364 × 184	250976
7	0.01875	(− 16.6125, − 8.325)	(− 13.05, 4.95)	190 × 708	134520
8	0.01875	(12.45, − 8.325)	(16.0125, 4.95)	190 × 708	134520
9	0.05625	(− 16.6125, − 14.5125)	(16.0125, − 8.2125)	580 × 112	64960
10	0.05625	(− 16.6125, 4.8375)	(16.0125, 11.1375)	580 × 112	64960
11	0.05625	(− 23.475, − 14.5125)	(− 16.5, 11.1375)	124 × 456	56544
12	0.05625	(15.9, − 14.5125)	(20.4, 11.1375)	80 × 456	36480
NACA	0.0001 *to* 0.0059	(− 0.071, − 0.135)	(1.2, − 0.135)	913 × 35	31955
Global		**(− 23.475, − 14.5125)**	**(20.4, 11.1375)**		**3284675**

Study4: Coarse Cartesian mesh + Coarse body mesh. This study is the same as Study1, but with coarser Cartesian mesh. The Cartesian mesh is made in order to have 6.5 cells in the vortex core radius. The global mesh is made of 227975 cells distributed as following:

Zone	Cell − egde	x_{min}, y_{min}	x_{max}, y_{max}	x × y	Cells
1	0.0750	(− 13.2, − 8.7)	(12.6, − 1.5)	344 × 96	33024
2	0.0250	(− 13.2, − 1.65)	(− 0.3, 0.)	516 × 66	34056
3	0.0250	(− 0.3, − 1.65)	(12.6, 0.)	516 × 66	34056
4	0.0250	(− 13.2, 0.)	(− 0.3, 1.65)	516 × 66	34056
5	0.0250	(− 0.3, 0.)	(12.6, 1.65)	516 × 66	34056
6	0.0750	(− 13.2, 1.5)	(12.6, 5.325)	344 × 51	17544
7	0.0750	(− 16.95, − 8.7)	(− 13.05, 5.325)	52 × 187	9724
8	0.0750	(12.45, − 8.7)	(16.35, 5.325)	52 × 187	9724
9	0.2250	(− 16.95, − 14.5125)	(16.35, − 8.2125)	148 × 28	4144
10	0.2250	(− 16.95, 4.8375)	(16.35, 11.1375)	148 × 28	4144
11	0.2250	(− 23.475, − 14.5125)	(− 16.5, 11.1375)	31 × 114	3534
12	0.2250	(15.9, − 14.5125)	(20.4, 11.1375)	20 × 114	2280
NACA	0.0017 *to* 0.0117	(− 0.068, − 0.135)	(1.2, 0.135)	449 × 17	7633
Global		**(− 23.475, − 14.5125)**	**(20.4, 11.1375)**		**227975**

2.4 JAXA computational domain

JAXA also conducted 4 corresponding studies as ONERA. Three layers of grid is used in JAXA computations as shown in figure 5. The grid spacing in the outer background is set to be the same as in ONERA zone C for each study. The inner background grid covers the whole vortex advection path and has the same grid spacing as in ONERA zone A. The width of the inner background grid is a little wider than ONERA zone A for better coverage of the vortex core. It is considered the corresponding studies in JAXA have the same grid resolutions with those in ONERA, so the differences in the results between each other for same study are from the differences of the numerical schemes and grid types and the geometry connectivity methods.

O-type grid is used for the NACA0012 profile in JAXA. For each study, points on the profile are kept at the same location as ONERA. The outer boundary is formed with an elliptic circle which covers nearly the same area as that of ONERA NACA0012 mesh with same bodywise points.

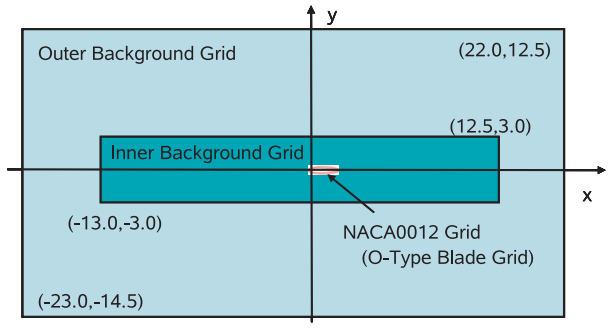

Figure 5: JAXA overlapped grids.

The boundary conditions for the outer background grid is setting a fixed inflow at the upstream boundary. For other 3 boundaries, zeroth order extrapolation is used to allow mass outflow without wave reflections. The outer boundaries are located far from the airfoil and there will be little influences on the solutions from the fixed inflow set at the upstream boundary.

2.5 ONERA choice of time steps for unsteady computations

The time-step has been set in order to highlight only the effects of the spatial discretization schemes. Taking into account the finest cell-edge length of the Cartesian grid, it has been set to following time steps so that the CFL number is 0.4 for the finest Cartesian grids.

-reference body and Cartesian grids (Study1 mesh): Δt = 0.005 for 2nd and high-order computations,

-refined body grid and reference Cartesian grids (Study2 mesh): Δt =0.005 for 2nd-order computation,

- refined body and Cartesian grids (Study3 mesh): Δt = 0.0025 for 2nd-order computation,

- coarse body and Cartesian grids (Study4 mesh): Δt = 0.01 for 2nd-order computation.

The computation is performed from t_0 = -10 to t_f = +10 so that the vortex passes under the blade leading edge at t= 0.

2.6 JAXA choice of time steps for unsteady computations

The global time steps for each study are the same as ONERA. The allowable time step for each grid is com-

puted according to the prescribed CFL numbers. If the global time step is smaller or equal to the allowable time step, then the global time step is used. If the global time step is greater than the allowable time step, then the divided time step which is smaller than the allowable time step is used. The sub-time integration steps is set as:

$$N_{substep} = INT\left(\frac{\Delta t_{global}}{\Delta t_{allowable}}\right) + 1.$$

The flowfield information of the blade grid is interpolated onto the inner background and then onto the outer background grid at each global time step. At each sub-time integration step inside the blade grid, the background flowfield is frozen and the outer boundary of the blade grid is interpolated from the background grid. For this case, only one sub-time step was required for the inner and outer background grid. For the blade grid, usually less than 10 steps are required. Note that the sub-time step numbers change depending on the flowfield itself to satisfy the CFL limits as stated in section 2.2..

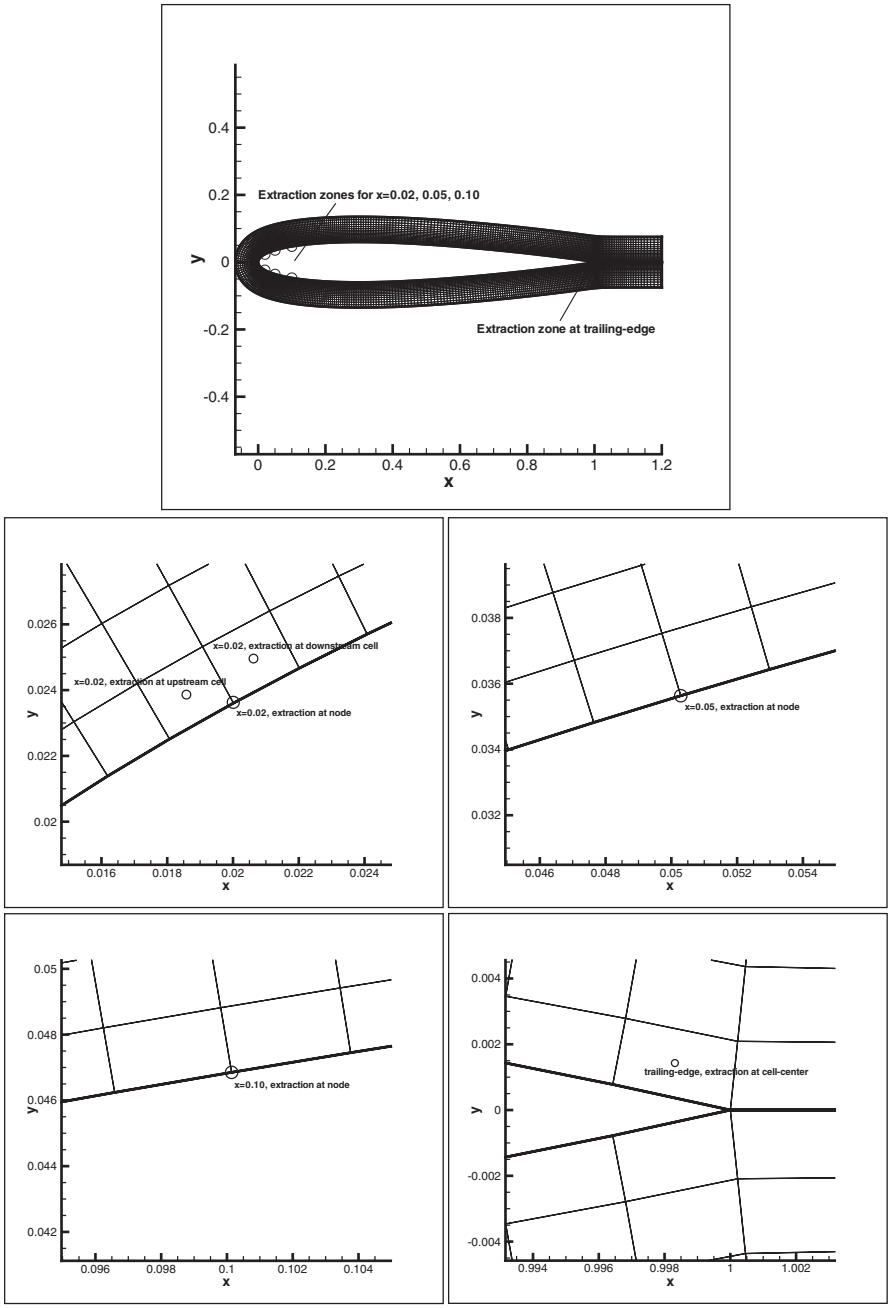

Figure 6: Location of the extraction nodes and cells for pressure values.

3 Data extraction

In order to compare and then evaluate the capability of respective JAXA and ONERA Euler methods for an accurate capture of main features of parallel Blade-Vortex Interaction, pressure is extracted from the body mesh on both upper and lower surfaces of the NACA0012 profile at:

- x = 0.02 on the NACA0012 profile (value at node) and at the center of the two adjacent cells (in order to check the quality of the value extrapolated at node),
- x = 0.05 on the NACA0012 profile (value at node),
- x = 0.1 on the NACA0012 profile (value at node),
- the center of the cell located at the trailing edge (in order to try to find out the origin of the vortex appearing at the trailing edge when the initial vortex passes underneath the trailing edge). Figure 6 represents the location of the extraction points on the upper part of the profile (the mesh being symmetrical with respect to $y = 0$) for studies 1 and 4 (reference NACA0012 mesh).

So far, only results at x = 0.02 will be compared, the features of the BVI being the most prominent at this point. The extraction point on the upper side of the profile is named point21, and on the one on the lower side of the profile is named *point* 31. In order to evaluate the numerical diffusion during the advection phasis of vortices, the vorticity on a horizontal line passing through the vortex center is extracted several times before the vortex reaches the airfoil (between t = -10 and t = -1).

4 ONERA and JAXA grid refinement studies

Here, the four meshes presented in section 2.3.5 are investigated for the ONERA 2nd-order and JAXA Euler methods.

First, a steady computation has been performed using numerical settings defined previously in section 2. A field corresponding to the Scully vortex is then superimposed to the steady solution to yield the initial condition of the unsteady computation.

4.1 Pressure coefficient distributions

4.1.1 Comparison of the 4 ONERA studies

Note: in the present figures, ONERA curves have been offset in order to cross NASA curve at t = -7.0.

Results for studies 1, 2, 3 and 4 are presented on figure 7. The *Cp* curves are almost the same for the 4 studies at both extraction points, except that the *Cp* values are slightly more important in Study4 when the vortex reaches the body. This seems unusual, as diffusion in Study4 is more important due to the use of a coarser grid. Seeking for the origin of this difference, it has been found out that the vortex moves towards the airfoil in all studies, because of the dispersal property of the numerical scheme, and this phenomenon seems to be much more important in Study4.

Study	**Vortex position at** t = -10.0	**Vortex position at** t = -1.0
1	(− 10.0; − 0.250)	(− 1.017; − 0.232)
2	(− 10.0; − 0.250)	(− 1.017; − 0.232)
3	(− 10.0; − 0.250)	(− 1.012; − 0.244)
4	(− 10.0; − 0.250)	(− 1.036; − 0.138)

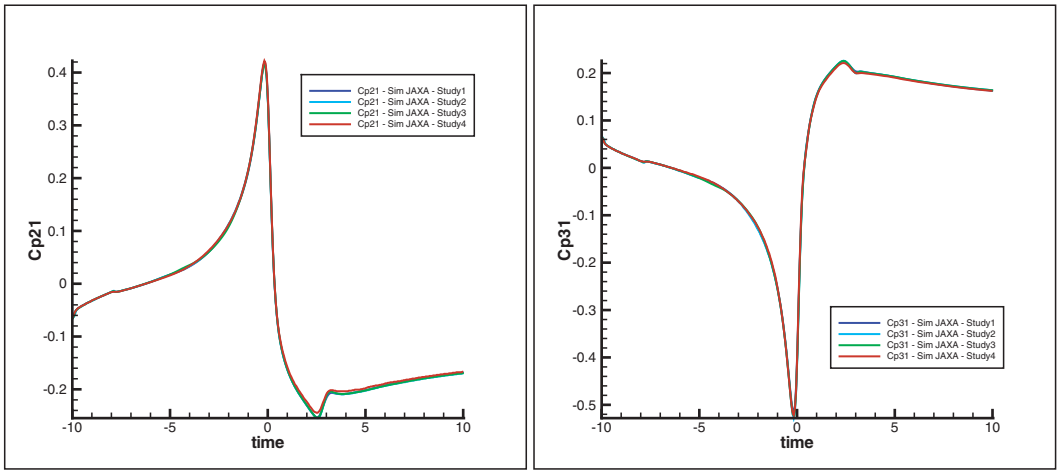

Figure 7: Cp at point 21 and 31, ONERA studies.

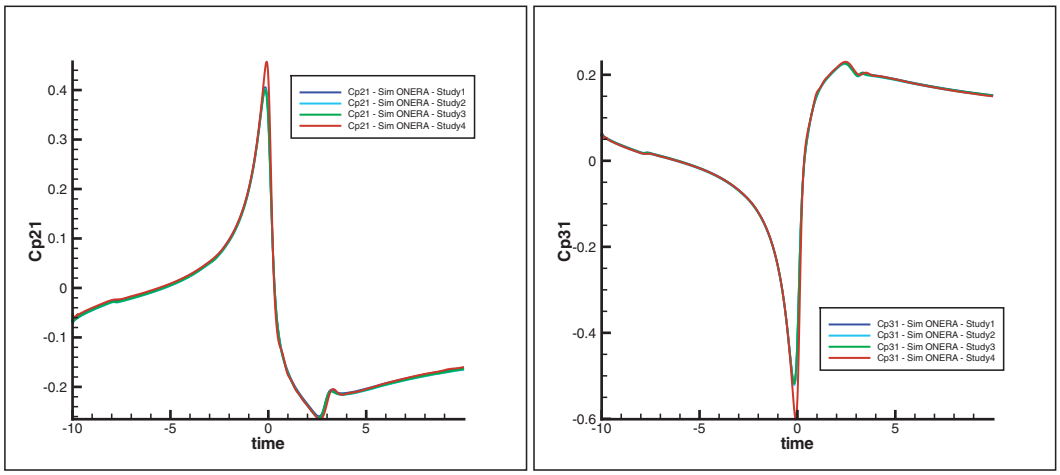

Figure 8: Cp4 at point 21 and 31, JAXA studies.

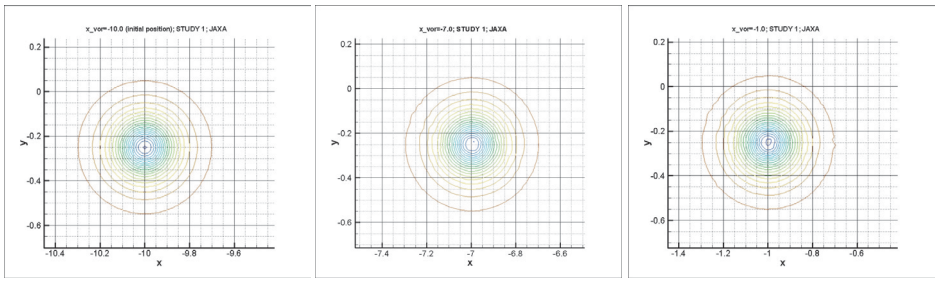

Figure 9: Vortex location at t=0, 3, 9 for JAXA Study1.

4.1.2 Comparison of the 4 JAXA studies

Note: in the present figures, JAXA curves have been offset in order to cross NASA curve at t = -7.0 (see below : Comparison of ONERA and JAXA studies versus NASA experiment).

Results for studies 1, 2, 3 and 4 are presented on figure 8. *Cp* levels at $t = 0$ for Study4 are the same as for other studies, and lower than the ones obtained with ONERA computations, probably because of numerical diffusion.

The vortex locations during the advection phasis in JAXA computations are also checked. Figure 9 shows the vortex location at times t=0, 3 and 9 for Study1. There is no movement of the vortex towards the profile.

4.1.3 Comparison of the 4 ONERA and JAXA studies versus NASA experiment

Note: in the present figures, JAXA and ONERA curves have been offset in order to cross NASA curve at t = -7.0.

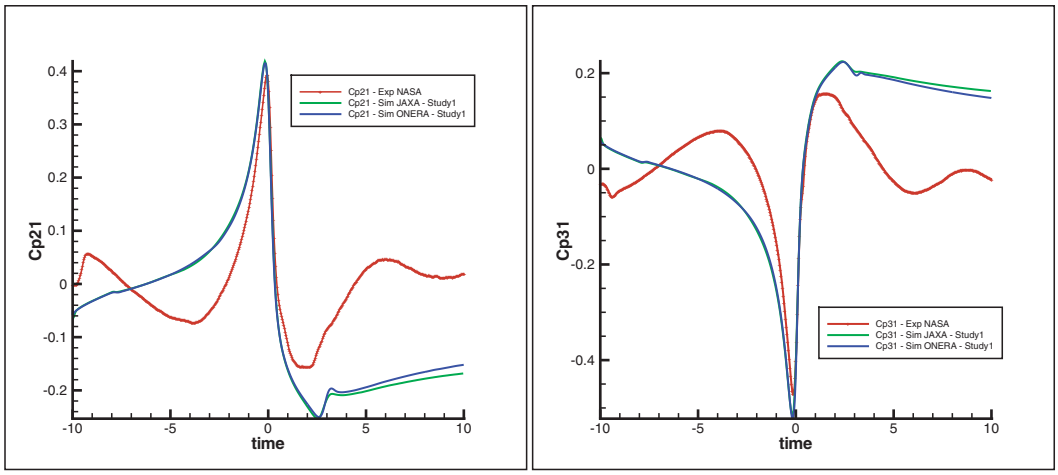

Figure 10: *Cp* at point 21 and 31, Study1.

As shown in figures 10, 11, 12, 13, for all studies, ONERA and JAXA results are quite identical for both extractions points, except for Study4 (coarsest mesh), in which JAXA results are better than ONERA results. Computational results are quite different from the NASA experimental results. This might be a consequence of 3D effects inherent to the experiment that are not simulated in our simulations. The *Cp* levels are satisfactory: the peak is well-appearing in computations. Future computations will have to check that the differences mainly result from 3D effects.

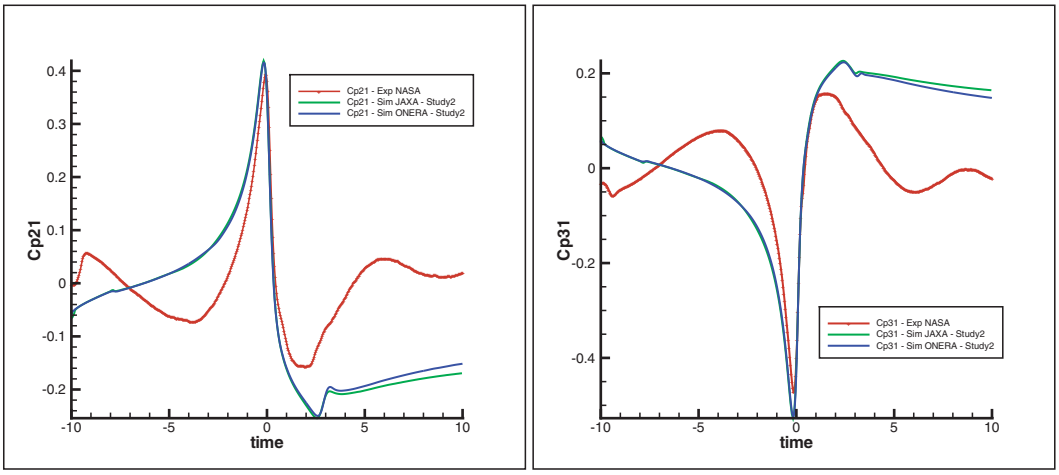

Figure 11: *Cp* at point 21 and 31, Study2.

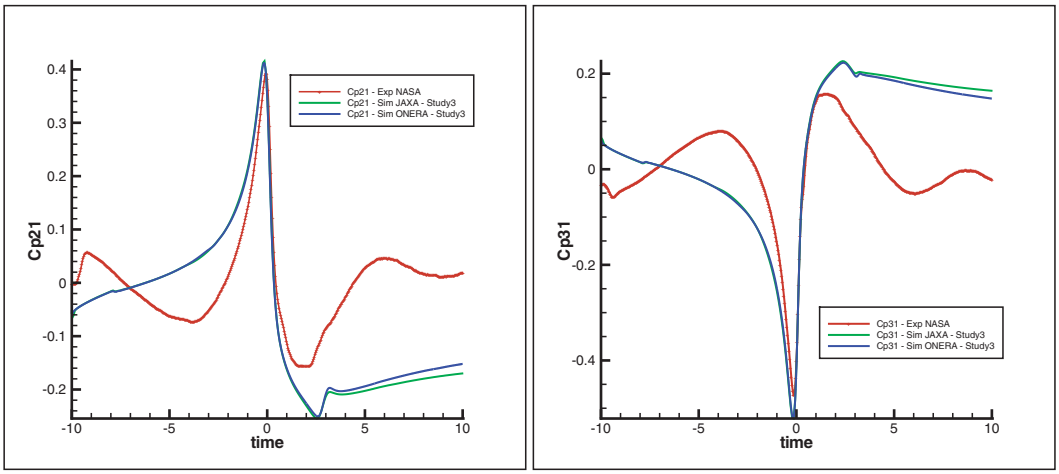

Figure 12: *Cp* at point 21 and 31, Study3.

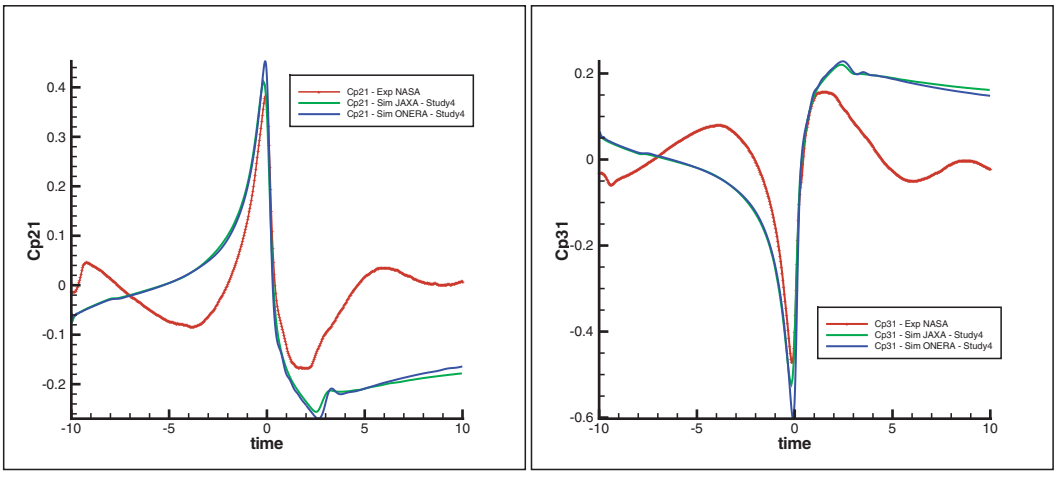

Figure 13: *Cp* at point 21 and 31, Study4.

At $t > 2$, there are some differences between ONERA and JAXA in the Cp curves. The reason for these differences may come from the different types of airfoil grid used, C-type for ONERA and O-type for JAXA. For C-type grid, the values at the cut line in the wake must be determined by some algebraic method, while for O-type grid, periodic solution is applied in the chordwise direction and the cut-line is treated same with other lines. Further discussion between JAXA and ONERA may be required to clarify this point.

4.2 Vorticity

Vorticity is defined as $\omega = \frac{\partial v}{\partial x} - \frac{\partial u}{\partial y}$ for this two-dimensional flow. The vorticity loss is evaluated at the vortex center where the vorticity reaches a maximum value as the ratio of the maximum value difference to the intial vortex maximum value.

4.2.1 Comparison of the 4 ONERA studies

Figure 14 compares the vorticity loss in the vortex core for studies 1, 3 and 4 with ONERA computations during the advection phasis.

The vorticity loss is very important in Study4, and quite acceptable in Study3. Thus, quantifying the vorticity loss between the moment when the vortex is introduced in the study (at x = -10) and the moment when the vortex approaches the airfoil (at x = -1), the vorticity losses are:

- 12% in Study1,
- 2% in Study3,
- 40% in Study4.

It is recalled that the vortex has to be kept during approximatively 100 chords for a 3D study, which means that less than 20% of the vortex vorticity is then lost if the mesh were as fine as in Study3. This would require a mesh of several million cells in the vortex core.

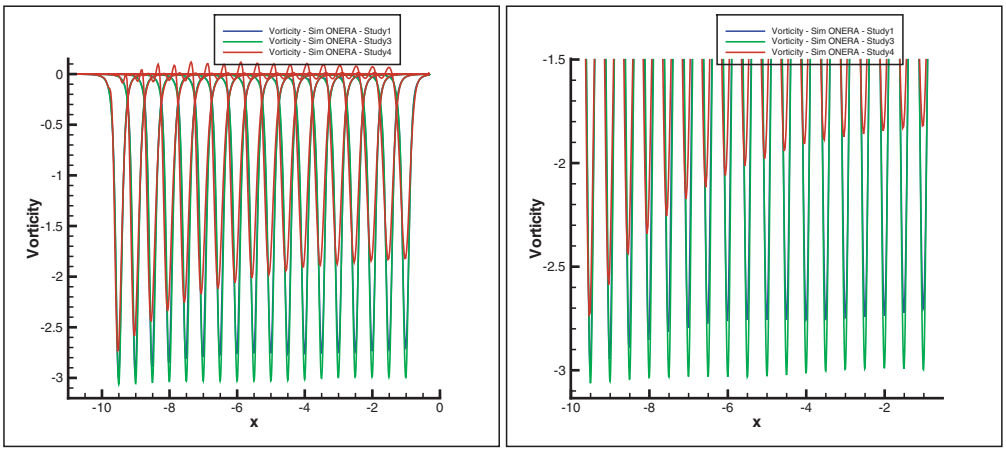

Figure 14: Vorticity, ONERA studies.

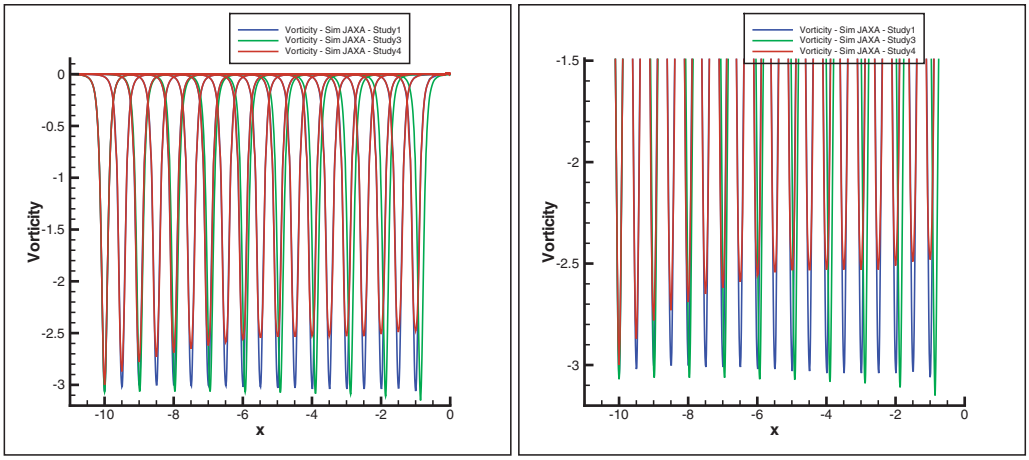

Figure 15: Vorticity, JAXA studies.

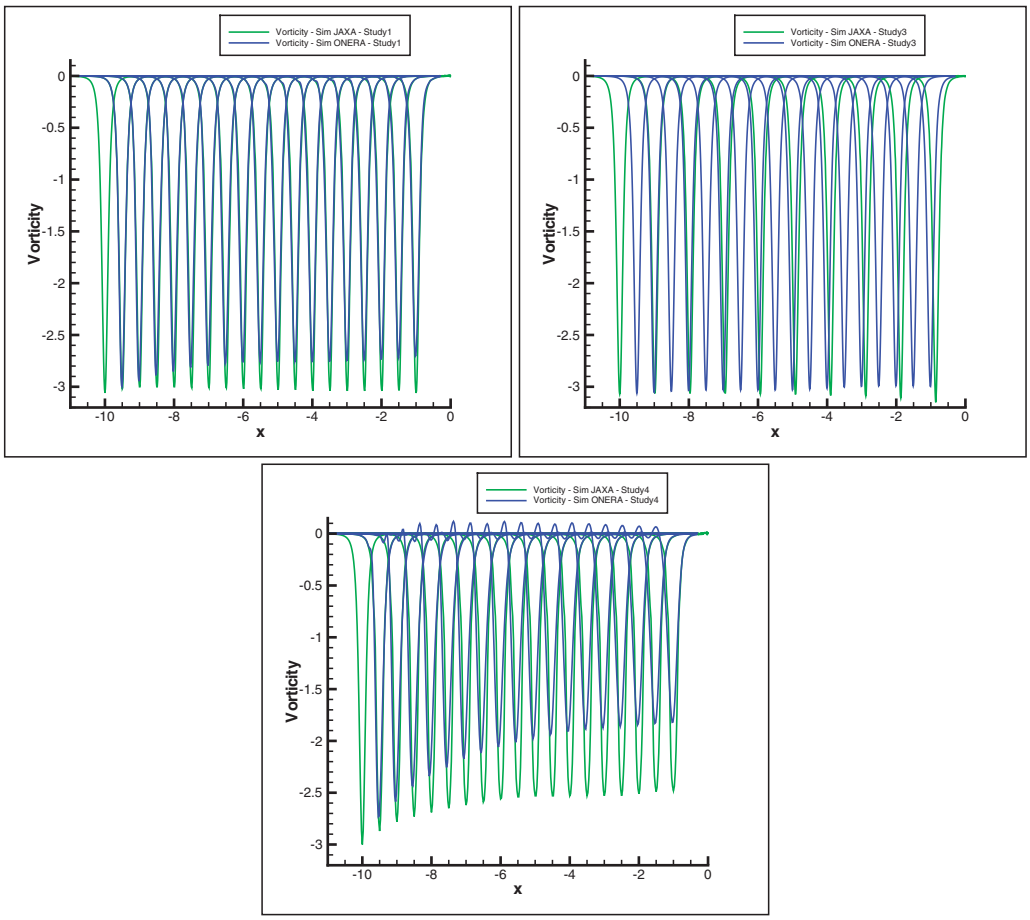

Figure 16: Vorticity, JAXA and ONERA studies 1, 3, 4.

4.2.2 Comparison of the 4 JAXA studies

Figure 15 compares the vorticity loss in the vortex core for studies 1, 3 and 4 with JAXA computations during the advection phasis. The vorticity losses are:

- 0 % in Study1,
- +1.5% in Study3,
- 16% in Study4.

The reason of the slight increase of vorticity in the finest grid case (Study3) is not well understood at this point. It may be due to the characteristic of the used SHUS scheme or because of the initial vortex is only an empirical one and is not in complete equilibrium with the Euler solver. There is no more increase while convected further downstream.

4.2.3 Comparison of ONERA studies versus JAXA studies

As seen in figure 16, the vorticity loss is lower for JAXA than for ONERA computations. JAXA results are satisfactory in studies 1 and 3, but the vorticity slightly increases in Study3, while the ONERA results are satisfactory only for Study3. Note the peak locations difference of JAXA computations are due to different sampling. There is no convection speed violation in either computation.

5 ONERA high-order studies on the reference mesh

So far only the reference mesh (first mesh in section 2.3.5 corresponding to Study1) is considered. Computations using 2nd, 3rd and 5th-order approaches (see section 2) are performed, using the ONERA Euler solver. ONERA high-order results are first compared to the 2nd-order results in order to highlight the accuracy improvement in terms of the vortex structure preservation. They are then compared to the NASA experiment and JAXA Study1 results.

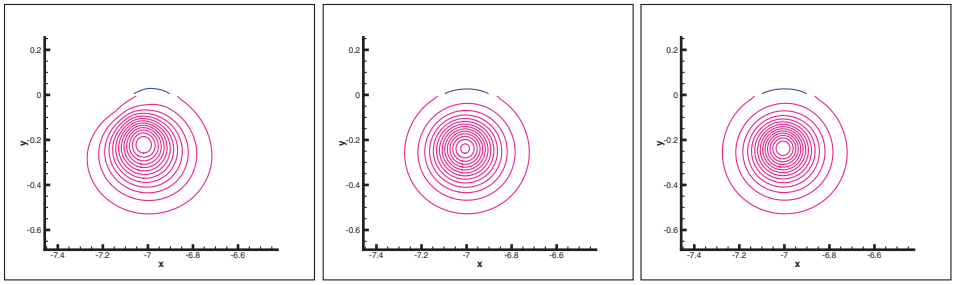

Figure 17: Vortex location at t = -7 for 2nd, 3rd and 5th-order computations.

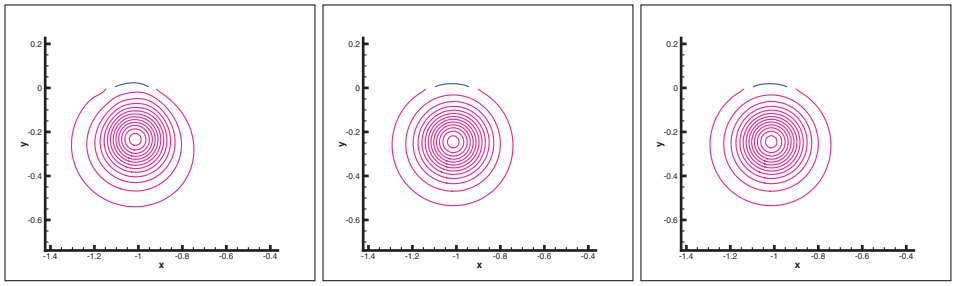

Figure 18: Vortex location at t = -1 for 2nd, 3rd and 5th-order computations.

5.1 Comparison of the vortex location during the advection phasis for high order computations

Figures 17 and 18 represent the vortex location at time t = -7 and t = -1 for 2nd, 3rd and 5th-order computations, during the advection phasis. The discontinuities on curves at the top of the vortex are due to the location of the matching boundary condition between grids 2 and 4 (see 2.3.2) and are only due to the postprocessing.

The vortex deviates from its initial position, namely y = -0.25, for the 2nd-order computation already at time t = -7, whereas it is well-located when applying higher-order schemes before passing under the leading edge of the profile.

5.2 Pressure coefficient distributions

5.2.1 Comparison of ONERA high-order studies with 2nd-order study

Cp curves at point 21 and 31 have a similar shape for 2nd, 3rd and 5th-order computations (figure 19).

5.2.2 Comparison of ONERA high-order studies versus JAXA study and NASA experiment

Note: in the present figures, JAXA and ONERA curves have been offset in order to cross NASA curve at t = -7.0. *Cp* curves at point 21 and 31 have a similar shape for ONERA high-order and JAXA computations before passing under the airfoil (figures 20 and 21). ONERA *Cp* curves present a rougher peak at t = 3 than the JAXA computation.

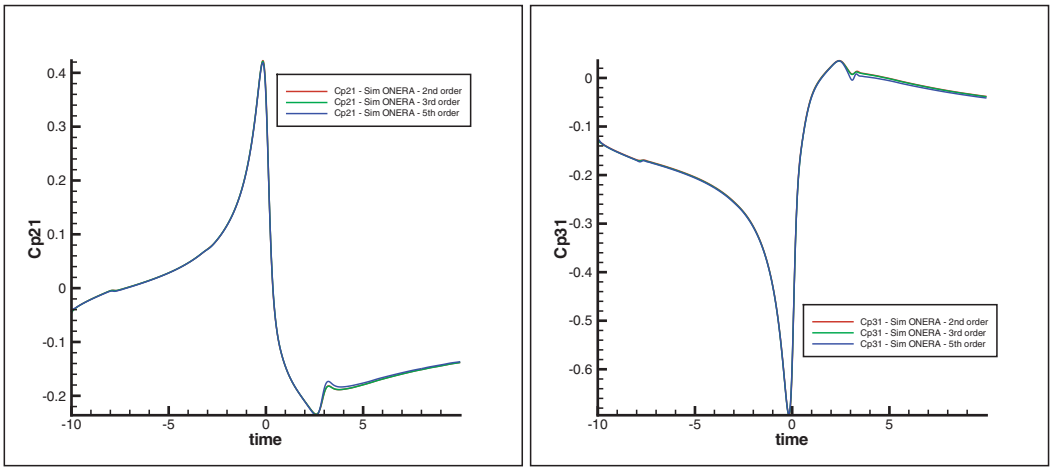

Figure 19: *Cp* at point 21 and 31, ONERA high-order studies.

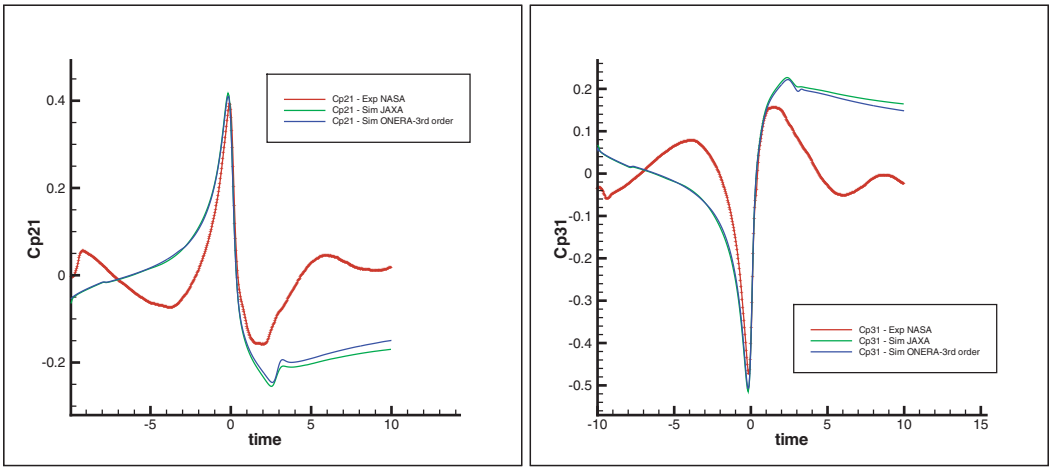

Figure 20: *Cp* at point 21 and 31, ONERA 3rd-order versus JAXA computations.

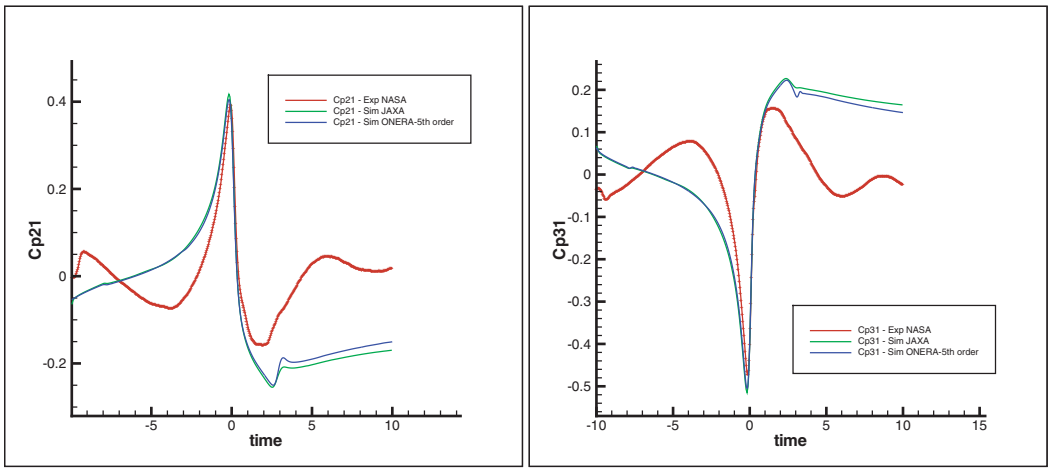

Figure 21: *Cp* at point 21 and 31, ONERA 5th-order versus JAXA computations.

5.3 Vorticity

5.3.1 Comparison of ONERA high-order studies with 2nd-order study

Figure 22 compares the vorticity slices in the vortex core for ONERA 2nd, 3rd and 5th-order computations during the advection phasis.

The vorticity loss is smaller for the 3rd-order computation than for the 2nd-order one at the beginning of the advection phasis of the vortex, and has then similar values for both schemes. This weak improvement can be explained by the fact that the artificial dissipation has the same formulation for both orders of accuracy.

The 5th-order computation yields a noticeable improvement of the vorticity preservation during the advection phasis. The vorticity loss is around 1.7% before the vortex reaches the airfoil leading edge, whereas it is around 10% for 2nd and 3rd-order computations.

5.3.2 Comparison of ONERA high order studies and JAXA first study

Figure 23 compares the vorticity in the vortex core for the reference mesh with ONERA high-order computations and JAXA computation before the vortex passes under the profile leading edge. The ONERA 5th-order computation presents now a satisfactory loss, comparable with JAXA numerical simulation.

Conclusion

Inviscid numerical simulations of two-dimensional parallel blade-vortex interaction are carried out in the framework of Task 1 (1st year) of the cooperative research activity between JAXA and ONERA on the “Comparison of CFD and BVI noise prediction methods for realistic rotors”. The capability of respective JAXA and ONERA Euler methods for an accurate capture of main features of

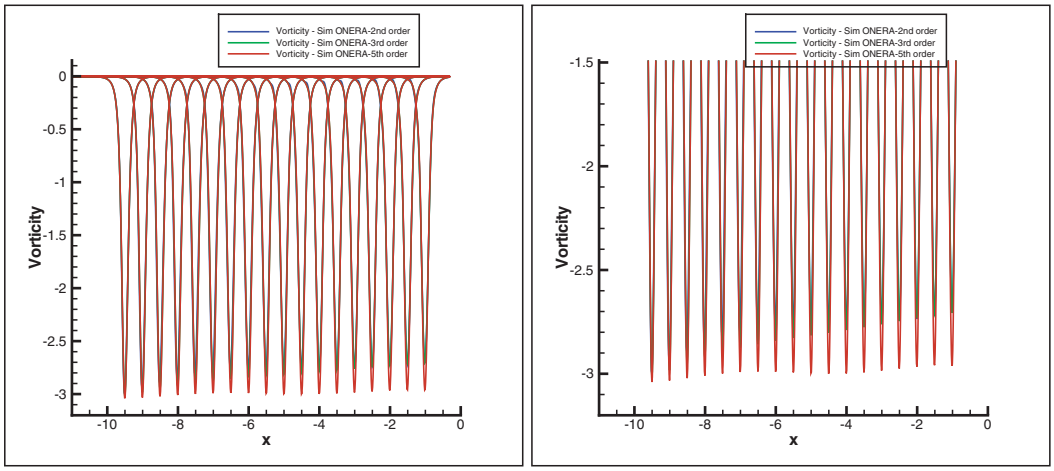

Figure 22: Vorticity, ONERA high-order studies.

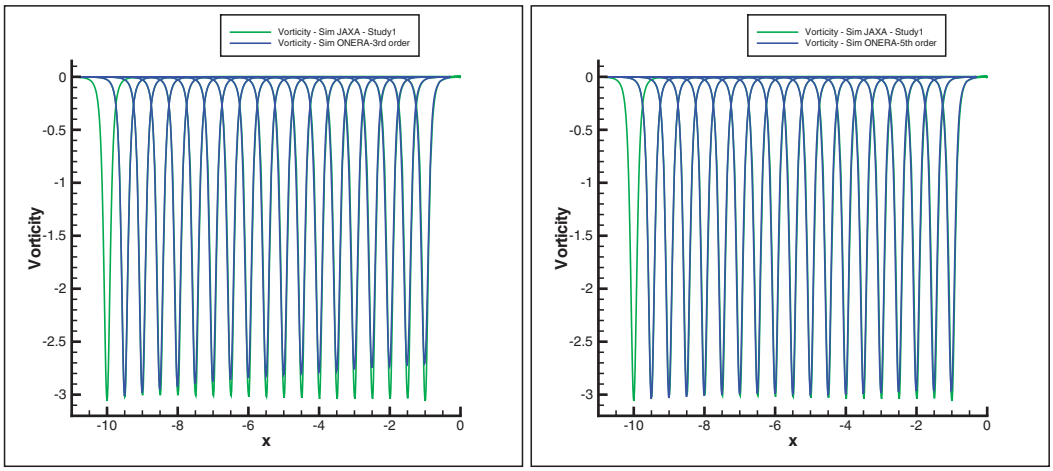

Figure 23: Vorticity, ONERA high-order versus JAXA computations.

parallel Blade-Vortex Interaction is evaluated. The results from each side are compared quite well to each other and with NASA experiments with the main features well captured. But some discripancies are found mainly due to different numerical schemes and computation approaches adapted by each organization.

A first study consisting in using different sizes of grids for ONERA 2nd-order approach and JAXA method has been performed. It appears that ONERA solver requires a fine Cartesian grid to minimize the vorticity loss during advection, whereas JAXA's allows for the use of a coarser grid, despite an slight increase of the vorticity for the latter.

In order to improve the vorticity preservation, 3rd and 5th-order computations have been performed by ONERA. On the reference mesh, the 5th-order computation yields a real improvement of the vorticity loss, as it reaches 1.7% of the initial vorticity before interacting with the profile, comparable with JAXA results.

References

[1] C. Kitaplioglu, F.X. Caradonna and C.L. Burley, Parallel blade-vortex interactions : an experimental study and comparison with computation, AHS, International Aeromechanics Specialists' Conference, 2nd - Aeromechanics Technology & Product Design for the 21st Century, Bridgeport, CT, Proceedings. Vol. 2; United States; 11-13 Oct. 1995. pp. 5-95 to 5-118.

[2] C. Kitaplioglu, F.X. Caradonna and M. McCluer, An Experimental Study of Parallel Blade-Vortex Interaction Aerodynamics and Acoustics Utilizing an Independently Generated Vortex, NASA/TM-1999-208790, 1999.

[3] J.F. Thompson, Z.U.A. Warsi, C.W. Mastin, Numerical grid generation : foundations and applications, Elsevier North-Holland, Inc. New York, NY, USA. 1985.

[4] C. Benoit, G. Jeanfaivre, E. Canonne, Synthesis of ONERA Chimera method developed in the frame of CHANCE program, 31st European Rotorcraft Forum, September 2005.

[5] C. Benoit, G. Jeanfaivre, 3D inviscid rotor and fuselage calculations using Chimera and automatic cartesian partitioning methods, Proceedings of the AHS Aeromechanics 2000, Atlanta, USA (2000).

[6] A. Lerat, J. Sides, V. Daru, An Implicit Finite-Volume Method for Solving the Euler Equations, Lecture Notes in Physics, vol. 170, pp. 343-349, 1982.

[7] A. Jameson, W. Schmidt, E. Turkel, Numerical Solutions of the Euler Equations by Finite Volume Method using Runge-Kutta Time Stepping Schemes, 1981, AIAA Paper 81-1259.

[8] A. Jameson, S. Yoon, Lower-upper implicit schemes with multiple grids for the Euler equations, 1987, AIAA Paper 0001-1452 vol.25 no.7 , pp. 929-935.

[9] A. Rezgui, P. Cinnella and A. Lerat, Third-Order Accurate Finite Volume Schemes for Euler Computations on Curvilinear Meshes, in Computer and Fluids, Volume 30, Issues 7-8, pp. 875-901, September 2001.

[10] O. Saunier et al., to be submitted at the 2007 ERF conference.

[11] A. Ochi, T. Aoyama, S. Saito, E. Shima, and E. Yamakawa, BVI Noise Predictions by Moving Overlapped Grid Method, 55th AHS Annual Forum, May 1999.

[12] E. Shima and T. Jounouchi, Role of CFD in Aeronautical Engineering (No.14)-AUSM Type Upwind Schemes, NAL SP-34, 1999, pp.7-12.

[13] H.C. Yee and A. Harten, Implicit TVD Schemes for Hyperbolic Conservation Laws in Curvilinear Coordinates, AIAA Journal, Vol. 25, No.2, February 1987, pp.266-274.

JAXA Research and Development Report JAXA-RR-06-042E

Date of Issue : 30 March, 2007
Edited and Published by : Japan Aerospace Exploration Agency
7-44-1 Jindaiji-higashimachi, Chofu-shi, Tokyo 182-8522, Japan
URL : http://www.jaxa.jp/
Printed by : Kyoushin Co., Ltd.